Pulmonary endothelial HIF2α-arginase axis plays an essential role in the development of hypoxia pulmonary hypertension

Andrew S. Cowburn, PhD[1,2]; Alexi Crosby, PhD[2]; David Macias, PhD[1]; Cristina Branco, PhD[1]; Renato Colaço, PhD[1]; Mark Southwood, PhD[3]; Mark Toshner, PhD[2] Laura E. Crotty Alexander, MD[4]; Nicholas W. Morrell, MD[2]; Edwin R. Chilvers, PhD[2]; and Randall S. Johnson, PhD[1]

Department of Physiology, Development and Neuroscience[1], Department of Medicine[2], University of Cambridge; Department of Pathology[3], Papworth Hospital NHS Foundation Trust; Division of Pulmonary and Critical Care[4], School of Medicine, University of California, San Diego

For correspondence: Dr. Andrew Cowburn or Professor Randall S. Johnson, Department of Physiology, Development and Neuroscience, University of Cambridge, Downing Street, Cambridge. CB2 3EG. United Kingdom, or.

E-mail: asc32@medschl.cam.ac.uk, or rsj33@cam.ac.uk

Short title: HIF2α is essential for pulmonary hypertension development

Keywords: HIF2α, arginase-1, pulmonary-endothelium, nitric oxide

Abstract

Hypoxic pulmonary vasoconstriction is correlated with pulmonary vascular remodelling. The hypoxia-inducible transcription factors (HIFs), HIF-1α and HIF-2α are known to contribute to the process of hypoxic pulmonary vascular remodelling; however, the specific role of pulmonary endothelial HIF expression in this process, and in the physiological process of vasoconstriction in response to hypoxia, remains unclear. Here we show that pulmonary endothelial HIF-2α is a critical regulator of hypoxia-induced pulmonary arterial hypertension (PAH). The rise in right ventricular systolic pressure (RVSP) normally observed following chronic hypoxic exposure was absent in mice with pulmonary endothelial HIF-2α deletion. The RVSP of mice lacking HIF-2α in pulmonary endothelium after exposure to hypoxia was not significantly different from normoxic wild type (WT) mice and much lower than the RVSP values seen in WT littermate controls and mice with pulmonary endothelial deletion of HIF-1α exposed to hypoxia. Endothelial HIF-2α deletion also protected mice from hypoxia remodelling. Pulmonary endothelial deletion of arginase-1, a downstream target of HIF-2α, likewise attenuated many of the pathophysiological symptoms associated with HPH.

We propose a mechanism whereby chronic hypoxia enhances HIF-2α stability, which causes increased arginase expression and dysregulates normal vascular NO homeostasis. These data offer new insight into the role of pulmonary endothelial HIF-2α in regulating the pulmonary vascular response to hypoxia.

Significance Statement

The expression of hypoxia inducible factor-(HIF)2a in pulmonary endothelium of mice influences pulmonary vascular resistance and development of hypoxic pulmonary hypertension (PH) via an arginase-1 dependent mechanism. The HIF-2a:arginase-1 axis influences the homeostatic regulation of nitric oxide synthesis in the lung. Impaired generation of this vasoactive agent contributes to the initial development and vascular remodelling process of PH.

\body

Introduction

Alveolar hypoxia affects vascular flow in the pulmonary vascular bed via an immediate vasoconstrictor response (hypoxic pulmonary vasoconstriction, or HPV) (1). This reduces perfusion of regions of the lung with lowered levels of air flow (2). In conditions including chronic obstructive pulmonary disease (3), idiopathic pulmonary fibrosis (4), and at high altitude (5), HPV probably contributes to persistent increases in pulmonary arterial pressures. This in turn is correlated with reduced plasticity of the vascular bed, sustained pulmonary vascular remodelling and, ultimately, debilitating right ventricular hypertrophy and failure(2).

The hypoxia inducible factors (HIFs) are transcription factors and key regulators of the molecular response to hypoxia. The targets of HIFs include genes controlling vascularization, cellular proliferation, migration, and metabolism(6-11). A well-characterized animal model of hypoxia-induced pulmonary hypertension involves exposure to chronic hypoxia (CH), typically 10-12% inspired oxygen. This results in extensive vascular remodelling,

marked pulmonary hypertension and right ventricular hypertrophy over a period of a few weeks. Exposure to CH in rodents results in vasoconstriction and a pattern of vascular remodelling that is reminiscent of humans with hypoxia-associated pulmonary hypertension (12, 13).

Mice that are hemizygous for either of the HIF isoforms, HIF-1α (14) or HIF-2α (15), have been shown to have attenuated pulmonary vascular remodelling following experimental CH. Conditional deletion of HIF-1α in smooth muscle also ameliorates the degree of remodelling in CH(16). The mechanisms by which HIF acts in pulmonary vascular remodelling are not fully defined; in particular, the role played by the endothelium in this process is not well understood. Here, we delete the HIF isoforms and one of their targets, the Arg1 gene, specifically in the pulmonary endothelium (17), and show that expression of the HIFα transcription factors in pulmonary endothelial cells is an essential aspect of the hypoxic response of the lung.

Results

Deletion of HIFα isoforms in pulmonary endothelium

Genetically manipulated mouse strains with conditional alleles of either the HIF-1α or -2α isoforms (18, 19) were crossed to mouse strains expressing the cre recombinase enzyme under the control of the pulmonary endothelium-specific Alk1- or L1 promoter (L1cre) (17). To determine tissue specificity of this transgene, we analysed the cre activity of adult L1cre mice by crossing with a ROSA26Sor$^{tm9(CAG\text{-}tdTomato)}$ reporter strain. As shown, lung vasculature

was easily identifiable. Minimal expression of tdTomato was detectable in the endothelium of other tissues (Supplemental Figure 1A). Deletion efficiency was assessed and deletion was greater than 80% (Supplemental Figure 1B), with little or no detectable deletion in other tissues.

HIF-2α deletion in the pulmonary endothelium prevents hypoxia-induced pulmonary hypertension

Wild type (WT) and pulmonary endothelial HIF-α deleted mice were exposed to normoxic or hypoxic (10% O_2) normobaric atmospheres for 21 days. Pulmonary hypertension was assessed through measurement of right ventricular systolic pressures (RVSPs) (Figure 1A). RVSP in L1cre-HIF-2α mice (18.9±1.0 mmHg, n=11) under normoxic conditions were significantly lower than littermate controls (22.4±1.1 mmHg, n=9, p=0.03) mice. However RVSP from normoxic L1cre-HIF-1α mice (24.7±1.7 mmHg, n=6) did not differ from WT controls (Figure 1A).

The RVSPs of L1cre-HIF-2α mice following hypoxic exposure (26.1±1.6 mmHg, n=7) were not significantly different from those of untreated WT mice (22.48±1.19, n=9) and were much lower than the elevated values seen in WT littermate controls (41.9±1.8 mmHg, n=12, p<0.0001) and L1cre-HIF-1α mice (36.25±2.37mmHg, n=7, p<0.005)(Figure 1A).

The ratio of right ventricular weights to those of the left ventricle plus septum (RV/LS+S), an indicator of right ventricular hypertrophy, was likewise significantly higher in wild-type (0.316±0.01, n=8, p<0.0001) and L1cre-HIF-1α (0.323±0.02, n=8, p<0.001) mice exposed to hypoxia compared to the ratios found in L1cre-HIF-2α (0.209±0.008, n=8) mice (Figure 1B). WT and

mutant mice reacted to hypoxia normally in other respects (Supplemental Figures 2A-2C).

Pulmonary endothelial HIF-2α is essential for vascular remodelling

Medial thickening of pulmonary vessels was calculated. Both WT littermates and L1cre-HIF-1α mice showed significantly increased medial thickness following hypoxic conditioning (Figure 1C). In comparison, hypoxic L1cre-HIF-2α mice showed a large relative reduction in medial thickness relative to WT animals. Normoxic animals showed no changes in vessel structure (Supplemental Figure 3).

Serial lung sections were immunostained to mark endothelial cells. Lungs from wild-type and L1cre-HIF-1α mice had typical tissue remodelling following chronic hypoxia (Figure 1D), with an increase in α-SMA associated with pulmonary arteries (Figure 1E). However, little to no remodelling was observed in lung sections from L1cre-HIF-2α mice (Figure 1F). Lung sections showed increases in elastin in both WT controls and L1cre-HIF-1α mice, but only minimal staining in the L1cre-HIF-2α mice (Figure 1D) (20). Collagen was also significantly higher in hypoxia-conditioned WT and L1cre-HIF-1α mice relative to L1cre-HIF-2α mice (Supplemental Figure 4A). Pulmonary endothelial deletion of HIF-2α reduced smooth muscle cell coverage after hypoxic exposure (Figure 1F). In comparison, both WT littermate control and L1cre-HIF-1α mice developed full and partial rings of α-SMA positive cells around vessels in hypoxia-conditioned animals (Figure 1F).

Reduced Arginase expression in HIF2α mutant mice

Previous work from our laboratory and others has demonstrated that the two HIFα isoforms act to control NO homeostasis during hypoxia. This occurs through HIF1α regulation of the NOS2/iNOS gene, and HIF-2α regulation of the Arg-1 and Arg-2 genes (21-25). The enzyme Arg-2 in particular has been implicated in reducing airway NO and promoting remodelling and collagen deposition in PAH patients (26, 27). We found that hypoxic up-regulation of arg-1 and -2 was reduced in hypoxia-conditioned isolated murine primary pulmonary endothelial cells (Supplemental Figure 5A) and whole lung samples from L1cre-HIF-2α mice, relative to WT littermate controls following hypoxic conditioning (Figure 2A).

Consistent with these data, we found that plasma $NO_{(X)}$ concentrations were significantly reduced in HIF-1α mice and elevated in HIF-2α mutant mice when compared to WT control mice (Figure 2B); this was mirrored in an increase in NO metabolites detected in whole lung extracts of hypoxically treated animals (Figure 2C). There was also an increase in exhaled NO detected in HIF-2α mutant mice (Figure 2D). Although several recent studies have highlighted the role of endothelin-1 (ET-1) in pulmonary hypertension and indicated its regulation by the HIF pathway, purified lung endothelial cells showed little change in ET-1 expression in this model (Supplemental Figures 5B-5D). There was a significant increase in PDGFβ expression in WT mice during the acute hypoxic phase (days1-3) before levels return to near baseline at the chronic phase (day 21). However there appears to be little separation between WT and L1cre-HIF2α mice (Supplemental Figure 6A-D). We further analyzed a number of stem cell markers known to be upregulated in PAH

(28). We found enhanced whole lung gene expression of both Oct3-4 and nanog in WT when compared to L1cre-HIF2α mice (Supplemental Figure 6E-H).

Pulmonary endothelial arginase-1 deletion attenuates PAH

We next sought to determine how the specific deletion of arginase-1 in the pulmonary endothelium influenced the development of PAH. The increase in RVSP normally observed following chronic hypoxic challenge (for WT mice, 41.7±0.8mm/Hg, n=7, $p<0.0001$) was significantly attenuated in mice with pulmonary endothelial arginase-1 deletion (31.2±1.0mmHg, n=7) (Figure 2E). Basal RVSPs in L1cre-arg1 mice under normoxia (23.0±0.7mmHg, n=6) were similar to those seen in littermate WT control mice (24.3±0.3mmHg, n=5). The ratio of right ventricular weight to left ventricle plus septum (RV/LS+S) was significantly higher in wild-type (0.39±0.01, n=6, $p<0.001$) when compared to L1cre-arg1 (0.33±0.01, n=9) mice, following chronic hypoxic exposure (Figure 2F); the animals otherwise responded normally to hypoxia (Supplemental Figure 7A). Wild type littermates showed significantly greater medial thickening (18.57%, n=15) when compared to L1cre-arg1 mice (14.35%, n=9) after exposure to chronic hypoxia (Figure 2G). Collagen deposition around the bronchial associated vasculature was significantly higher in hypoxically conditioned WT control mice relative to L1cre-arg1 mice (Supplemental Figure 4B).

L1cre-arg1 mice showed substantially less α-SMA associated with pulmonary arteries in close proximity to terminal bronchioles when compared to wild type controls (Supplemental Figure 7B). Staining for α-SMA was also substantially

reduced in the peripheral pulmonary vasculature of these mutants (Figure 2H-I). Deletion of pulmonary endothelial arg-1 significantly elevated plasma $NO_{(x)}$ relative to the levels seen in plasma from wild type control mice (Figure 2J).

Changes in acute response to hypoxia caused by loss of endothelial HIF-2α

Hypoxia rapidly stimulates pulmonary vascular resistance (HPV), and increases the pressure needed to maintain normal output from the right ventricle of the heart. We compared HPV in WT control and mutant animals by measuring right ventricular systolic pressures (RVSP), both immediately before and during hypoxic challenge (method shown in Figure 3A). L1cre-HIF-2α mice have a lower resting RVSP (18.99±1.00mmHg, n=11) than WT control animals (22.47±1.19mmHg, n=9)(Figure 1A); nonetheless, the magnitude of pressure changes induced by hypoxia were still significantly lower in mice lacking pulmonary endothelial HIF-2α (3.10±0.60mmHg, n=13) relative to that seen in WT animals (5.45±0.76mmHg, n-13 p=0.023). RVSP recorded from L1cre-HIF-1α (4.56±1.53mmHg, n=7) mice, however, did not significantly deviate from WT controls (Figure 3B) during acute hypoxic exposure. Thus, acute pressure changes in the pulmonary circulation induced by hypoxia are significantly lower in animals that lack HIF-2α in the pulmonary endothelium. Baseline arterial saturations for L1cre-HIF-2α mice did not deviate from wild-type controls (Figure 3C). However during the acute hypoxic challenge, there was a strong trend towards greater desaturation in the L1cre-HIF-2α when compared to WT mice (Figure 3C, p=0.06, n=7).

Whole-body plethysmography showed that resting ventilation rates in normoxia are similar in the HIFα mutant animals relative to WT controls (WT control 168±3.0 breaths per minute (BrPM), L1cre-HIF-1α 174±2.8 BrPM and L1cre-HIF-2α 170±2.7 BrPM)(Figure 3D). All mice responded to acute hypoxia by increasing ventilation rates. L1cre-HIF-1α and WT littermate control mice increased to 258 and 250 BrPM respectively for the initial 5 minutes before reducing their ventilation rates to 187 and 174 BrPM during the first hour of exposure to hypoxia. However, L1cre-HIF-2α mice increased respiratory rate to 308 BrPM, then reduced their ventilation rates to 233 BrPM in the same time period (Figure 3D). Of note, both tidal volume and peak inhalation/exhalation flow rates are comparable between the three groups (Supplemental Figure 8 A, B and C), indicating that there is no anatomic difference in pulmonary capacity. The carotid bodies in all animals were histologically normal (Supplemental Figure 8D-H).

Endothelial progenitor cells from human PAH patients have altered HIF-2α-dependent arginase expression

Blood outgrowth endothelial cells (BOECs) have been extensively used as a model for studying in-vitro endothelial function in vascular disorders (29, 30) with close functional and gene expression similarity to pulmonary artery endothelial cells(31).

Previous work has shown enhanced expression and activity of Arg-2 in PAH patients (27, 32). As shown here by Western blotting, no defect in hypoxia-driven stability of HIF-1α and HIF-2α expression in these cells and confirm the normoxic over-expression at mRNA and protein and activity of Arg-2 in these

cells (Fig 4A and Supplemental Fig 9A and B). Hypoxia further increases the expression of Arg-2 in these BOECs from PAH patients.

BOEC's from control volunteers produce significantly more NO than BOECs from PAH patients following 48 hours in culture (Supplemental Fig 9C). NO production was restored to near that seen in control BOECs following arginase inhibition with S-(2-boronoethyl)-L-cysteine (BEC) (Supplemental Fig 9C). Short-hairpin (sh)RNA technology was employed to specifically knock-down HIF-1α, HIF-2α, and Arg-2 in these BOECs. These data show that knock-down of HIF-2α suppresses the expression of Arg-2 (Figure 4B) and decreases Arg-2 enzyme activity in these cells from patients with PAH (Figure 4C).

Discussion

In this study, we have shown that the endothelial cell is a necessary element in the changes that result in PAH, and that the HIF isoform HIF-2α is in turn required for that endothelial response. We also observed the down-regulated expression of arginase in isolated pulmonary endothelial cells and whole lungs from L1cre-HIF2a mice following chronic hypoxia, and demonstrate here that deletion of arginase-1 specifically in the pulmonary endothelium attenuated the development of hypoxic pulmonary hypertension. Given the role of HIF-2α in regulating arginases specifically, this indicates that a key aspect of the function of HIF-2α in PAH is its regulation of arginase expression.

The HIF pathway was implicated in PH initially through demonstrations showing that mice hemizygous for HIF-1α or HIF-2α have diminished levels of pulmonary hypertension (15, 33); subsequent work was able to show that hemizygosity for HIF-1α resulted in changes in myocyte hypertrophy and polarization(14). In contrast, hemizygosity of HIF-2α revealed that endothelial changes resulting in PAH were partially blocked when HIF-2α was diminished(15). Recent studies have also shown that PHD2 loss, which gives rise to increased HIF protein stability, promotes a HIF-2α-dependent increase in pulmonary hypertension(34, 35). These studies further demonstrate the importance of the HIF pathway in the etiology of PAH.

The causal link between pulmonary hypertension and NO homeostasis has been extensively documented (26, 36), and this is reflected clinically in the finding that intrapulmonary nitrates, biochemical reaction products of NO in bronchoalveolar fluid, and exhaled NO are all diminished in human pulmonary hypertension (37, 38). Interestingly, primary pulmonary endothelial cells isolated from PAH patients have substantially increased expression of arg-2 (27), which would be predicted to decrease available L-arginine and reduce NOS-derived NO formation. We have previously shown that both Arg1 and Arg2 are HIF-2α-dependent genes, and we show here that their expression in pulmonary endothelium is decreased in HIF-2α pulmonary endothelium mutants. This should result in an increase in pulmonary endothelial NO, which itself has been shown to alleviate PAH experimentally (39). Consistent with this hypothesis, genetic deletion of arg-1 resulted in a marked attenuation in the pathologies associated with PAH. Given a mechanistic link between

these findings and the etiology of PAH, future therapies to manipulate the control of NO homeostasis by the HIFα pathway should certainly be explored.

Methods

Animals. All animals were housed in an Association and Accreditation of Laboratory Animal Care International-approved facility. All protocols and surgical procedures were approved by the local and national animal care committees. Targeted deletion of HIF-1α, HIF-2α and arginase-1 in pulmonary endothelial cells was created by crossing (C57Bl6/j) homozygous for the floxed allele in HIF-1α, HIF-2α or arginase-1 into a background of Cre recombinase expression drive by the L1 (alk-1) promoter kindly donate by Dr Paul Oh, Florida University.(17) Mice characterized as wild type (WT) were in all cases littermates of respective mutant mice, homozygous for conditional alleles but without the cre recombinase transgene.

Measurement of Right Ventricular Systolic Pressure (RVSP). For induction of PAH due to chronic hypoxia, groups of male mice (8-12 weeks) were maintained in a normobaric hypoxic chamber (FiO_2 10%) for up to 21 days. Mice were weighed then anesthetised (isoflurane) and right-sided heart catheterisation through the right jugular using a pressure-volume loop catheter (Millar).(40-42) Bloods were taken for haemodynamic assessment.

Right Ventricular Hypertrophy. To measure the extent of right ventricular hypertrophy (RVH), the heart was removed and the right ventricule (RV) free wall was dissected from the left ventricle plus septum (LV+S), and weighed separately.(43) The degree of RVH was determined from the ratio RV/LV+S.

Tissue Preparation. In all animals the left lung was fixed *in situ* in the distended state by the infusion of 0.8% agarose into the trachea, and then placed in 10% paraformaldehyde before paraffin embedding. The right lung was frozen in liquid nitrogen for mRNA extraction.

Pulmonary Vascular Morphometry. Detailed methods in supplemental material and methods online.

Haematological Analysis. Anti-coagulated blood was analysed using Vet abc haematology analyser (Horiba) according to the manufacturers instructions.

Nitrite/Nitrate Analysis. Blood samples were centrifuged to separate plasma and were passed through a column with a 10-kDa cut-off filter. All samples were analysed for total $NO_{(X)}$ content using a NOA 280i (Siever, GE Healthcare) according to the manufacturers instructions.

RNA Analysis. Detailed methods in supplemental material and methods online.

Blood outgrowth endothelial cells (BOEC) isolation culture.

BOECs have been extensively used as a model for studying in-vitro endothelial function in vascular disorders (29, 30) and we have previously demonstrated their close functional and gene expression similarity to pulmonary artery endothelial cells(31). BOECs were isolated as previously

described (44). BOECs were isolated from peripheral blood was taken from consenting healthy volunteers at the Addenbrooke;s University of Cambridge teaching Hospital NHS Foundation Trust, Cambridge, UK following a protocol approved by the Cambridge (UK) Research Ethics Committee (REF:11/EE/0297). Detailed methods in supplemental material methods online.

Arginase activity assay

BOECs were prepared in lysis buffer for an arginase activity assay as previously described (45). Detailed methods in supplemental material and methods online.

Carotid Body Histology. Carotid body histology was performed as previously reported(46). Carotid body volume and cell numbers were quantified on microscope images (Leica DM-RB) using ImageJ software. Detailed methods in supplemental material methods online.

Whole Body Unrestrained Plethysmography. A single chamber plethysmograph (Data Science) was used in conjunction with a pressure transducer. Non-anesthetized mice were randomly placed into the plethysmograph and allowed to acclimate, once acclimated to the chamber, the composition of the flow gas was switched from 21% O_2 to 10% O_2 using a PEGAS mixer (Columbus instruments). Detailed methods in supplemental material and methods online.

Exhaled Nitric Oxide analysis

Exhaled nitric oxide was measured non-invasively in non-anesthetised mice using a closed chamber system as previously described (47). Briefly, gas phase NO was measured by a chemiluminescence-based NO analyser sensitive to 0.1ppb NO (NOA 280i Sievers, Boulder CO). Detailed methods in supplemental material and methods online.

Primary Lung endothelial cell isolation

Primary endothelial cells were isolated and cultured from lungs of L1cre-HIF2α and wt mice, as previously described(25). Detailed methods in supplemental material and methods online.

Knockdown experiments.

Human blood outgrowth endothelial cells derived from both control and PAH donors were transduced using lentiviral particles containing three different short hairpin RNAs (shRNAs) targeting human HIF-1α, HIF-2α, and Arg-2 mRNA, respectively. Detailed methods in supplemental material and methods online.

Statistical Analysis. All data represents the mean ($\pm$SEM) of *n* separate experiments unless otherwise stated. Difference between groups were assessed using *t* test unless otherwise stated. A *p* value of <0.05 was considered significant.

Acknowledgement. We thank Dr Paul Oh from Department of Physiology and Functional Genomics, University of Florida for providing the L1(alk-1)cre mouse.

Funding Sources

This study was funded by The Wellcome Trust, Papworth Hospital NIHR Cambridge Biomedical Research Centre.

Disclosures

None.

References

1. von Euler US, Liljestrand, G. (1946) Observations on the pulmonary arterial blood pressure in the cat. *Acta Physiologica Scand* 12:19.
2. Sylvester JT, Shimoda LA, Aaronson PI, & Ward JP (2012) Hypoxic pulmonary vasoconstriction. *Physiol Rev* 92(1):367-520.
3. Naeije R (2005) Pulmonary hypertension and right heart failure in chronic obstructive pulmonary disease. *Proc Am Thorac Soc* 2(1):20-22.
4. Lettieri CJ, Nathan SD, Barnett SD, Ahmad S, & Shorr AF (2006) Prevalence and outcomes of pulmonary arterial hypertension in advanced idiopathic pulmonary fibrosis. *Chest* 129(3):746-752.
5. Bartsch P & Gibbs JS (2007) Effect of altitude on the heart and the lungs. *Circulation* 116(19):2191-2202.
6. Semenza GL (2003) Targeting HIF-1 for cancer therapy. *Nature reviews. Cancer* 3(10):721-732.
7. Semenza GL (2009) Regulation of vascularization by hypoxia-inducible factor 1. *Ann N Y Acad Sci* 1177:2-8.
8. Pouyssegur J, Dayan F, & Mazure NM (2006) Hypoxia signalling in cancer and approaches to enforce tumour regression. *Nature* 441(7092):437-443.
9. Formenti F, *et al.* (2010) Regulation of human metabolism by hypoxia-inducible factor. *Proceedings of the National Academy of Sciences of the United States of America* 107(28):12722-12727.
10. Djagaeva I & Doronkin S (2010) Hypoxia response pathway in border cell migration. *Cell Adh Migr* 4(3):391-395.
11. Hubbi ME, *et al.* (2014) Cyclin-dependent kinases regulate lysosomal degradation of hypoxia-inducible factor 1alpha to promote cell-cycle progression. *Proceedings of the National Academy of Sciences of the United States of America* 111(32):E3325-3334.
12. Stenmark KR, Meyrick B, Galie N, Mooi WJ, & McMurtry IF (2009) Animal models of pulmonary arterial hypertension: the hope for etiological discovery and pharmacological cure. *American journal of physiology. Lung cellular and molecular physiology* 297(6):L1013-1032.
13. Dickinson MG, Bartelds B, Borgdorff MA, & Berger RM (2013) The role of disturbed blood flow in the development of pulmonary arterial hypertension: lessons from preclinical animal models. *American journal of physiology. Lung cellular and molecular physiology* 305(1):L1-14.
14. Shimoda LA, Manalo DJ, Sham JS, Semenza GL, & Sylvester JT (2001) Partial HIF-1alpha deficiency impairs pulmonary arterial myocyte electrophysiological responses to hypoxia. *American journal of physiology. Lung cellular and molecular physiology* 281(1):L202-208.
15. Brusselmans K, *et al.* (2003) Heterozygous deficiency of hypoxia-inducible factor-2alpha protects mice against pulmonary hypertension and right ventricular dysfunction during prolonged hypoxia. *The Journal of clinical investigation* 111(10):1519-1527.

16. Ball MK, *et al.* (2014) Regulation of hypoxia-induced pulmonary hypertension by vascular smooth muscle hypoxia-inducible factor-1alpha. *American journal of respiratory and critical care medicine* 189(3):314-324.
17. Park SO, *et al.* (2008) ALK5- and TGFBR2-independent role of ALK1 in the pathogenesis of hereditary hemorrhagic telangiectasia type 2. *Blood* 111(2):633-642.
18. Ryan HE, *et al.* (2000) Hypoxia-inducible factor-1alpha is a positive factor in solid tumor growth. *Cancer Res* 60(15):4010-4015.
19. Gruber M, *et al.* (2007) Acute postnatal ablation of Hif-2alpha results in anemia. *Proc Natl Acad Sci U S A* 104(7):2301-2306.
20. Yamataka T & Puri P (1997) Pulmonary artery structural changes in pulmonary hypertension complicating congenital diaphragmatic hernia. *J Pediatr Surg* 32(3):387-390.
21. Melillo G, *et al.* (1995) A hypoxia-responsive element mediates a novel pathway of activation of the inducible nitric oxide synthase promoter. *J Exp Med* 182(6):1683-1693.
22. Louis CA, *et al.* (1998) Distinct arginase isoforms expressed in primary and transformed macrophages: regulation by oxygen tension. *The American journal of physiology* 274(3 Pt 2):R775-782.
23. Takeda N, *et al.* (2010) Differential activation and antagonistic function of HIF-{alpha} isoforms in macrophages are essential for NO homeostasis. *Genes & development* 24(5):491-501.
24. Cowburn AS, *et al.* (2013) HIF isoforms in the skin differentially regulate systemic arterial pressure. *Proceedings of the National Academy of Sciences of the United States of America* 110(43):17570-17575.
25. Branco-Price C, *et al.* (2012) Endothelial cell HIF-1alpha and HIF-2alpha differentially regulate metastatic success. *Cancer cell* 21(1):52-65.
26. Grasemann H, *et al.* (2015) Arginase inhibition prevents bleomycin-induced pulmonary hypertension, vascular remodeling, and collagen deposition in neonatal rat lungs. *American journal of physiology. Lung cellular and molecular physiology* 308(6):L503-510.
27. Xu W, *et al.* (2004) Increased arginase II and decreased NO synthesis in endothelial cells of patients with pulmonary arterial hypertension. *FASEB journal : official publication of the Federation of American Societies for Experimental Biology* 18(14):1746-1748.
28. Firth AL, Yao W, Remillard CV, Ogawa A, & Yuan JX (2010) Upregulation of Oct-4 isoforms in pulmonary artery smooth muscle cells from patients with pulmonary arterial hypertension. *American journal of physiology. Lung cellular and molecular physiology* 298(4):L548-557.
29. Toshner M, *et al.* (2009) Evidence of dysfunction of endothelial progenitors in pulmonary arterial hypertension. *American journal of respiratory and critical care medicine* 180(8):780-787.
30. Wang JW, *et al.* (2013) Analysis of the storage and secretion of von Willebrand factor in blood outgrowth endothelial cells derived from patients with von Willebrand disease. *Blood* 121(14):2762-2772.
31. Toshner M, *et al.* (2014) Transcript analysis reveals a specific HOX signature associated with positional identity of human endothelial cells. *PloS one* 9(3):e91334.

32. Chu Y, *et al.* (2016) Arginase inhibitor attenuates pulmonary artery hypertension induced by hypoxia. *Mol Cell Biochem* 412(1-2):91-99.
33. Yu AY, *et al.* (1999) Impaired physiological responses to chronic hypoxia in mice partially deficient for hypoxia-inducible factor 1alpha. *The Journal of clinical investigation* 103(5):691-696.
34. Dai Z, Li M, Wharton J, Zhu MM, & Zhao YY (2016) PHD2 Deficiency in Endothelial Cells and Hematopoietic Cells Induces Obliterative Vascular Remodeling and Severe Pulmonary Arterial Hypertension in Mice and Humans through HIF-2alpha. *Circulation*.
35. Kapitsinou PP, *et al.* (2016) The Endothelial Prolyl-4-Hydroxylase Domain 2/Hypoxia-Inducible Factor 2 Axis Regulates Pulmonary Artery Pressure in Mice. *Molecular and cellular biology* 36(10):1584-1594.
36. Machado RF, *et al.* (2004) Nitric oxide and pulmonary arterial pressures in pulmonary hypertension. *Free radical biology & medicine* 37(7):1010-1017.
37. Girgis RE, *et al.* (2005) Decreased exhaled nitric oxide in pulmonary arterial hypertension: response to bosentan therapy. *American journal of respiratory and critical care medicine* 172(3):352-357.
38. Kaneko FT, *et al.* (1998) Biochemical reaction products of nitric oxide as quantitative markers of primary pulmonary hypertension. *American journal of respiratory and critical care medicine* 158(3):917-923.
39. Budts W, *et al.* (2000) Aerosol gene transfer with inducible nitric oxide synthase reduces hypoxic pulmonary hypertension and pulmonary vascular remodeling in rats. *Circulation* 102(23):2880-2885.
40. Crosby A, *et al.* (2011) Praziquantel reverses pulmonary hypertension and vascular remodeling in murine schistosomiasis. *American journal of respiratory and critical care medicine* 184(4):467-473.
41. Crosby A, *et al.* (2010) Pulmonary vascular remodeling correlates with lung eggs and cytokines in murine schistosomiasis. *American journal of respiratory and critical care medicine* 181(3):279-288.
42. Crosby A, *et al.* (2015) Hepatic Shunting of Eggs and Pulmonary Vascular Remodeling in Bmpr2(+/-) Mice with Schistosomiasis. *American journal of respiratory and critical care medicine* 192(11):1355-1365.
43. Morrell NW, Atochina EN, Morris KG, Danilov SM, & Stenmark KR (1995) Angiotensin converting enzyme expression is increased in small pulmonary arteries of rats with hypoxia-induced pulmonary hypertension. *The Journal of clinical investigation* 96(4):1823-1833.
44. Ormiston ML, *et al.* (2015) Generation and Culture of Blood Outgrowth Endothelial Cells from Human Peripheral Blood. *J Vis Exp* (106):e53384.
45. Zhang C, *et al.* (2004) Upregulation of vascular arginase in hypertension decreases nitric oxide-mediated dilation of coronary arterioles. *Hypertension* 44(6):935-943.
46. Macias D, Fernandez-Aguera MC, Bonilla-Henao V, & Lopez-Barneo J (2014) Deletion of the von Hippel-Lindau gene causes sympathoadrenal cell death and impairs chemoreceptor-mediated adaptation to hypoxia. *EMBO Mol Med* 6(12):1577-1592.
47. Le-Dong NN, *et al.* (2012) Measuring exhaled nitric oxide in animal models: methods and clinical implications. *J Breath Res* 6(4):047001.

Figure Legends

Figure 1. Pulmonary endothelial HIF-2α contributes to chronic hypoxic pulmonary hypertension. (A) Scatter plot (mean ± SEM) of right ventricular systolic pressure (RVSP). Wild-type (WT) and L1cre-HIFα mice were housed in normoxia (N) or chronic hypoxia (H) (WT (N) n=9 (H) n=12; L1cre-HIF-1α (N) n= 6 (H) n=7; L1cre-HIF-2α (N) n=11 (H) n=7). (B) Right ventricular hypertrophy. Scatter plot (mean ± SEM) show RV/LV+S weight ratio in mice exposed to normoxia (N) or chronic hypoxia (H) (WT (N) n=9 (H) n=12; L1cre-HIF-1α (N) n= 6 (H) n=7; L1cre-HIF-2α (N) n=11 (H) n=7). (C and D) Airway remodelling in wild-type (WT) (n=15), L1cre-HIF-1α (n=7) and L1cre-HIF-2α (n=7) post-chronic hypoxic challenge. (C) Scatter plot (mean ± SEM) of pulmonary vessel medial thickness. Quantification of the intimal medial thickness achieved by staining lung sections with EVG. (D) Histological sections immunostained with α–smooth-muscle actin(α-SMA), von Willebrand factor(vWF), and Elastic van Gieson (EVG). Representative photomicrographs (200μM bar) demonstrate lack of remodelling in L1cre-HIF-2α pulmonary arteries associated with terminal bronchi. Loss of HIF-2α in pulmonary endothelial cells reduces the degree of muscularization of peripheral arteries. (E) Stacked bar chart showing muscularization of peripheral pulmonary arteries in lung sections (blue bar = full muscle ring, green bar = partial muscle ring, yellow bar = no muscle ring) from wild-type (WT) (n=15), L1cre-HIF-1α (n=9) and L1cre-HIF-2α (n=7) mice. (F) Representative photomicrographs (100μM bar) immunostained for α-smooth muscle (arrows point to distal vessels). *P<0.05, **P<0.001, ***P<0.0001

Figure 2. Endothelial deletion of HIF-2α maintains higher plasma nitrate levels. (A) qPCR analysis of arginase-I/-II, NOS2, and VEGF mRNA from whole lung samples of wild-type (WT) (open bar, n=7), L1cre-HIF-1α (blue bar, n=7) and L1cre-HIF-2α (red bar, n=6). (B) Total nitric oxide in plasma and (C) whole lung by the conversion of $NO_{(X)}$ to NO using a nitric oxide analyser (Siever). Data shown as scatter plot with mean ± SEM from WT (n=7), L1cre-HIF-1α (n=7) and L1cre-HIF-2α (n=6) post chronic hypoxia challenge. Whole lung lysate analysis for $NO_{(X)}$ in normoxic (C) wt (open bar n=7), L1cre-HIF2α □□□□□□□□ n=7) L1cre-Arg1 (green bar n=4) and following chronic hypoxia (10% O_2 21-days), wt (white checker n=16) L1cre-HIF2α □□□□□checker □□□ n=7) L1cre-Arg1 (green checker bar n=9). Exhaled nitric oxide was measured non-invasively in non-anesthetised mice in normoxia (D) gas phase NO was measured by a chemiluminescence-based NO analyser (Carrier gas baseline 1.7ppb dotted line). Data shown as bar graph with mean ± SEM for normoxic WT (n=13), and L1cre-HIF-2α (n=8) and L1-Arg1(n=5). Pulmonary endothelial deletion of Arg-1 attenuates hypoxic pulmonary hypertensive phenotype. (E) Scatter plot (mean ± SEM) shows the effect of pulmonary endothelial Arg-1 on right ventricular systolic pressure (RVSP). Wild-type (WT) and L1cre-Arg1 mice were housed in normoxia (N) or chronic hypoxia (H) (WT (N) n=5 (H) n=7; L1cre-Arg1 (N) n= 6 (H) n=7. (F) Effect of pulmonary endothelial Arg-1 on right ventricular hypertrophy. Scatter plot (mean ± SEM) show RV/LV+S weight ratio in mice exposed to normoxia (N) or chronic hypoxia (H) (WT (N) n=6 (H) n=6; L1cre-Arg1 (N) n= 7 (H) n=9. (G) Airway remodelling was determined in wild-type (WT) (n=8), L1cre-Arg1 (n=10). Quantification of the intimal medial thickness. (H) Stacked bar chart showing the degree of muscularization of peripheral pulmonary arteries in lung sections from

wild-type (WT) (n=5), L1cre-Arg1 (n=6) mice. (I) Representative photomicrographs (100μM bar) immunostained for α-smooth muscle actin showing near and complete ring formation in peripheral vessel of WT mice when compared to L1cre-Arg1 mice. (J) Total nitric oxide was determined in the plasma by the conversion of NO_x to NO using a nitric oxide analyser (Siever). Data shown as scatter plot with mean ± SEM from WT (n=6), L1cre-Arg1 (n=8) post chronic hypoxia challenge *P<0.05, **P<0.001, ***P<0.0001.

Figure 3. Acute hypoxic pulmonary vasoconstriction is significantly blunt in L1cre-HIF-2α mutants. (A) Line diagram showing the time line and gas composition used to determine the acute hypoxic pulmonary vasoconstriction response. (B) Acute hypoxic pulmonary vasoconstriction was determined by measuring RVSP before and during acute hypoxic challenge (10% O_2). The delta between the two pressures was determined as the hypoxic vasoconstriction response. Data shown in bar graph as mean ± SEM from wild-type (WT) (n=13) L1cre-HIF-1α (n=7) and L1cre-HIF-2α (n=13). (C) Percentage arterial oxygen saturation was recorded during the acute hypoxic challenge. Data recorded at 5 sec intervals mean ± SEM of wild-type (n=7) and L1cre-HIF-2α (n=7) (D) Ventilation rate in response to acute hypoxia was determined by whole-body plethysmography. Resting/normoxic ventilation was determined 60 minutes prior to acute hypoxic stimulus. Data shown as mean breaths per minute ± SEM for WT (n=10) L1cre-HIF-1α (n=5) and L1re-HIF-2α (n=6). *P<0.05

Figure 4. Analysis of human blood out-growth endothelial Cells (BOECs) as a model for studying in-vitro endothelial function in pulmonary arterial hypertension

(PAH). (A) Western blot analysis of HIF1α and HIF2α stability and arginase-2 expression in normoxia and 16hr post hypoxia. Data shown in bar graph as a ratio of target gene to β-actin, mean ± SEM of control (closed bar n=3) and PAH (red bar n=4). (B) A lentiviral short-hairpin RNA strategy was employed to target HIF1α, HIF2α and Arg-2 expression. Three shRNA were used to knock-down each gene of interest. A scramble-sh and GFP-tagged lentivirus and no-treatment were included as controls. Data shown (mean ± SEM qPCR fold change compared to no-treatment control) for Arg-2 from control (closed bar, n=3) and PAH (red bar, n=3) 16hr post hypoxia. (C) Cell lysates were analysed for arginase activity following the shRNA strategy to knock-down HIF1α, HIF2α and Arg-2. Data shown as mean ± SD of urea produced corrected per mg of protein lysate for control (closed bar n=2) and PAH (red bar n=2). *P<0.05, **P<0.001 (control) *P<0.05, **P<0.001(PAH).

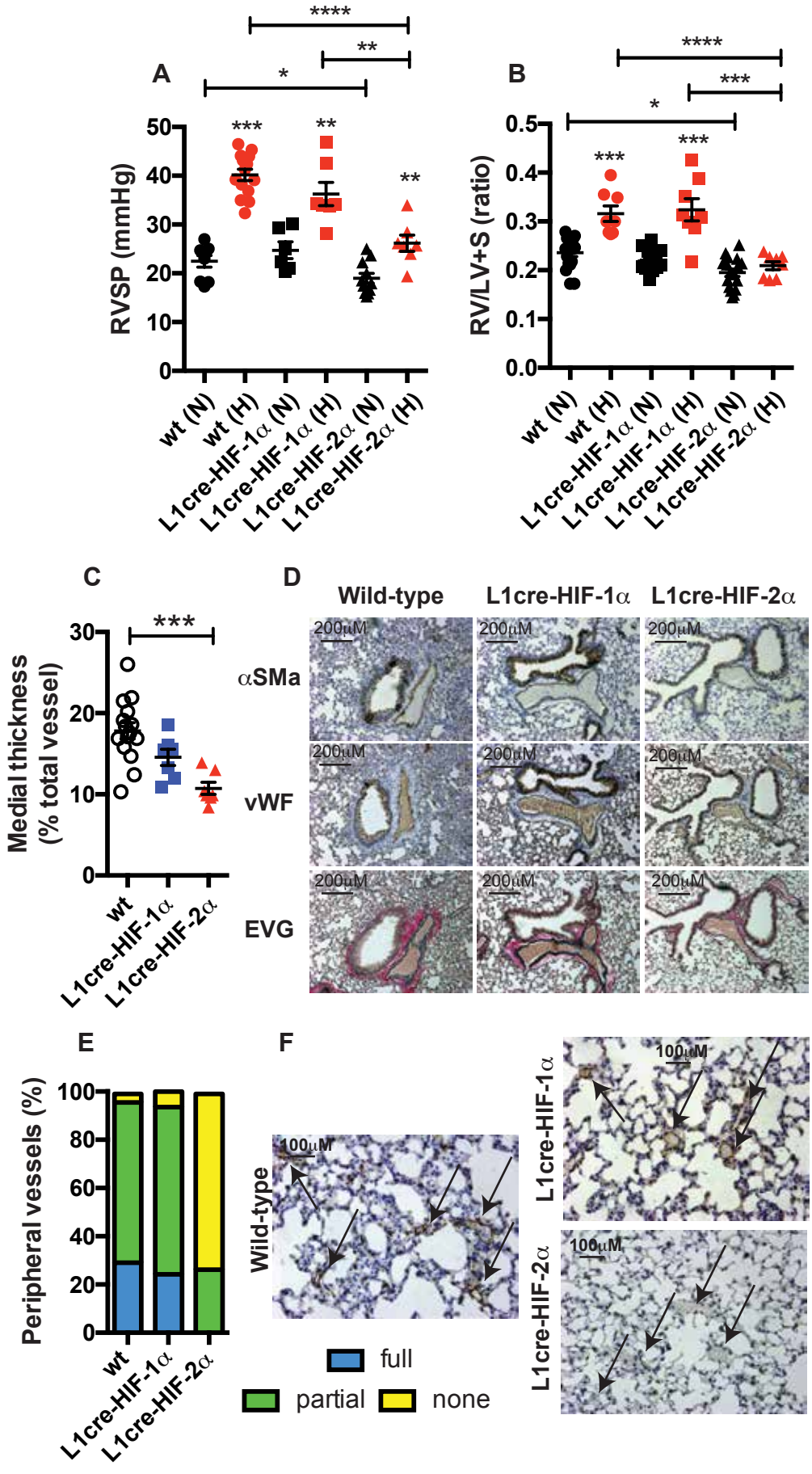
A
B
C
D
E
F
RVSP (mmHg)
RV/LV+S (ratio)
Medial thickness (% total vessel)
Peripheral vessels (%)
wt (N)
wt (H)
L1cre-HIF-1α (N)
L1cre-HIF-1α (H)
L1cre-HIF-2α (N)
L1cre-HIF-2α (H)
wt
L1cre-HIF-1α
L1cre-HIF-2α
Wild-type
L1cre-HIF-1α
L1cre-HIF-2α
αSMa
vWF
EVG
200μM
100μM
full
partial
none

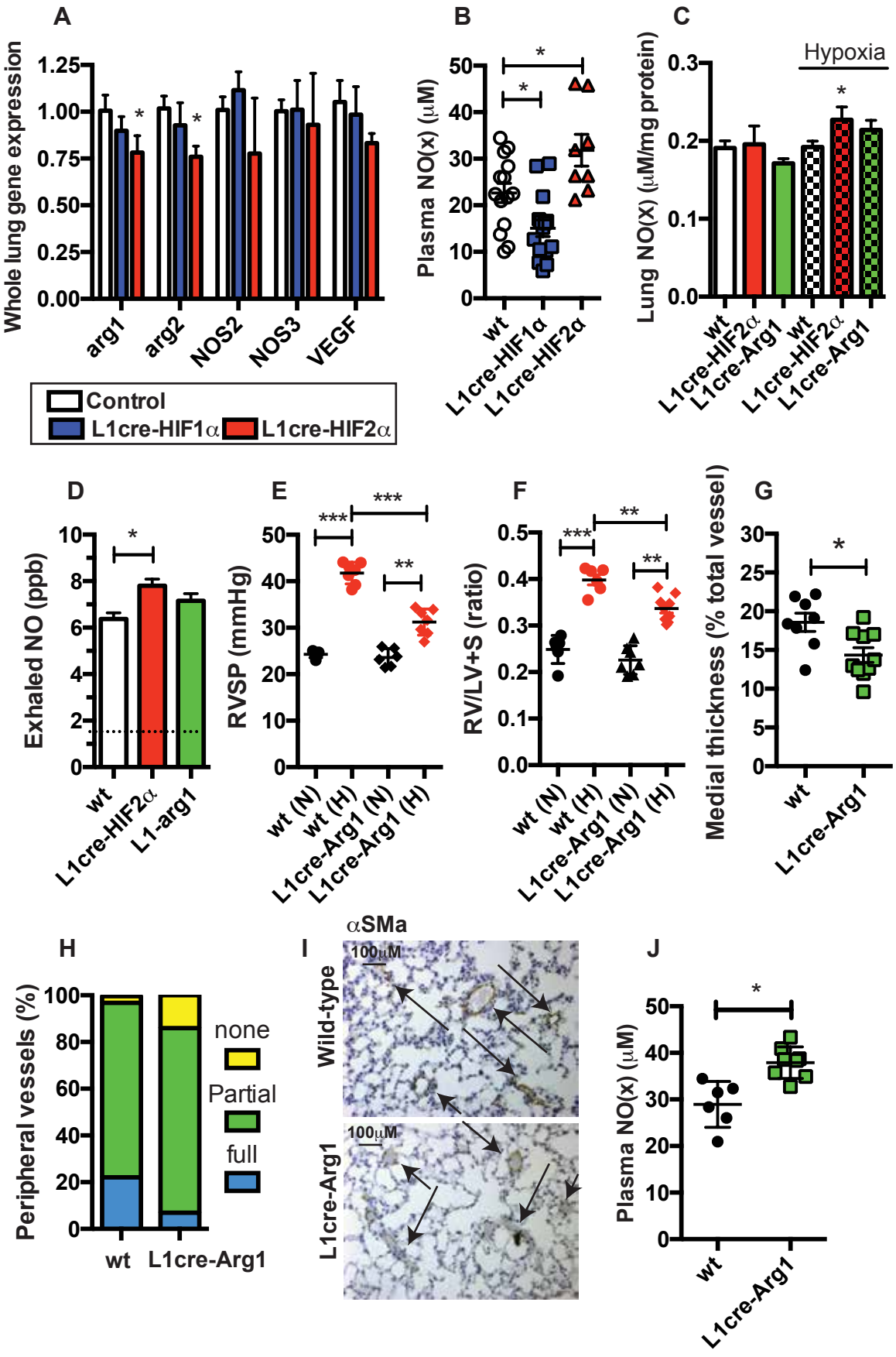
A
Whole lung gene expression
1.25
1.00
0.75
0.50
0.25
0.00
arg1
arg2
NOS2
NOS3
VEGF
Control
L1cre-HIF1α
L1cre-HIF2α
B
Plasma NO(x) (μM)
50
40
30
20
10
0
wt
L1cre-HIF1α
L1cre-HIF2α
C
Hypoxia
Lung NO(X) (μM/mg protein)
0.3
0.2
0.1
0.0
wt
L1cre-HIF2α
L1cre-Arg1
wt
L1cre-HIF2α
L1cre-Arg1
D
Exhaled NO (ppb)
10
8
6
4
2
0
wt
L1cre-HIF2α
L1-arg1
E
RVSP (mmHg)
50
40
30
20
10
0
wt (N)
wt (H)
L1cre-Arg1 (N)
L1cre-Arg1 (H)
F
RV/LV+S (ratio)
0.5
0.4
0.3
0.2
0.1
0.0
wt (N)
wt (H)
L1cre-Arg1 (N)
L1cre-Arg1 (H)
G
Medial thickness (% total vessel)
30
25
20
15
10
5
0
wt
L1cre-Arg1
H
Peripheral vessels (%)
100
80
60
40
20
0
none
Partial
full
wt
L1cre-Arg1
αSMa
I
Wild-type
L1cre-Arg1
100μM
100μM
J
Plasma NO(x) (μM)
50
40
30
20
10
0
wt
L1cre-Arg1

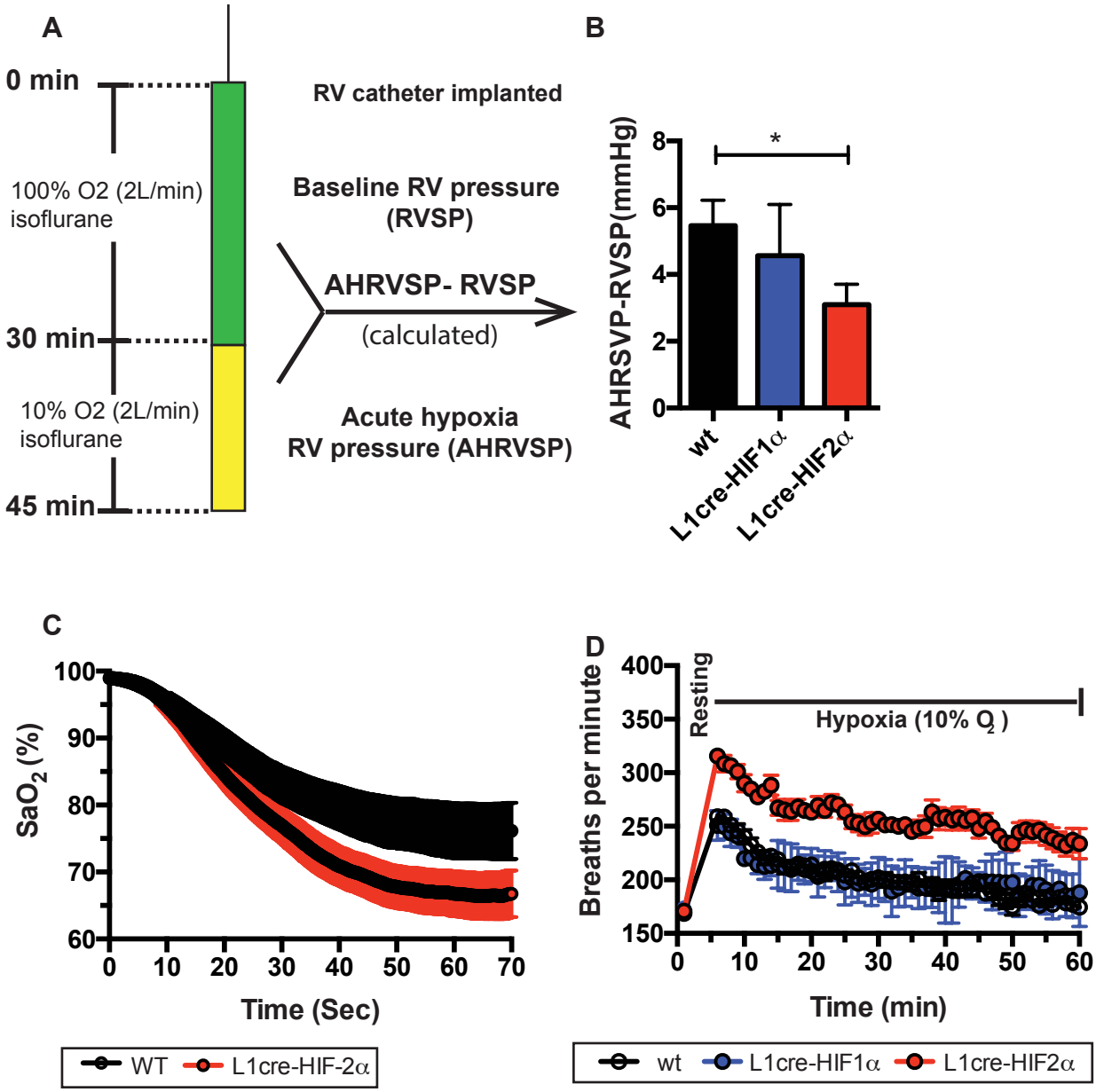
A
0 min
RV catheter implanted
100% O2 (2L/min)
isoflurane
Baseline RV pressure
(RVSP)
AHRVSP- RVSP
(calculated)
30 min
10% O2 (2L/min)
isoflurane
Acute hypoxia
RV pressure (AHRVSP)
45 min
B
AHRSVP-RVSP(mmHg)
8
6
4
2
0
*
wt
L1cre-HIF1α
L1cre-HIF2α
C
SaO2 (%)
100
90
80
70
60
0
10
20
30
40
50
60
70
Time (Sec)
WT
L1cre-HIF-2α
D
Breaths per minute
400
350
300
250
200
150
Resting
Hypoxia (10% O2)
0
10
20
30
40
50
60
Time (min)
wt
L1cre-HIF1α
L1cre-HIF2α

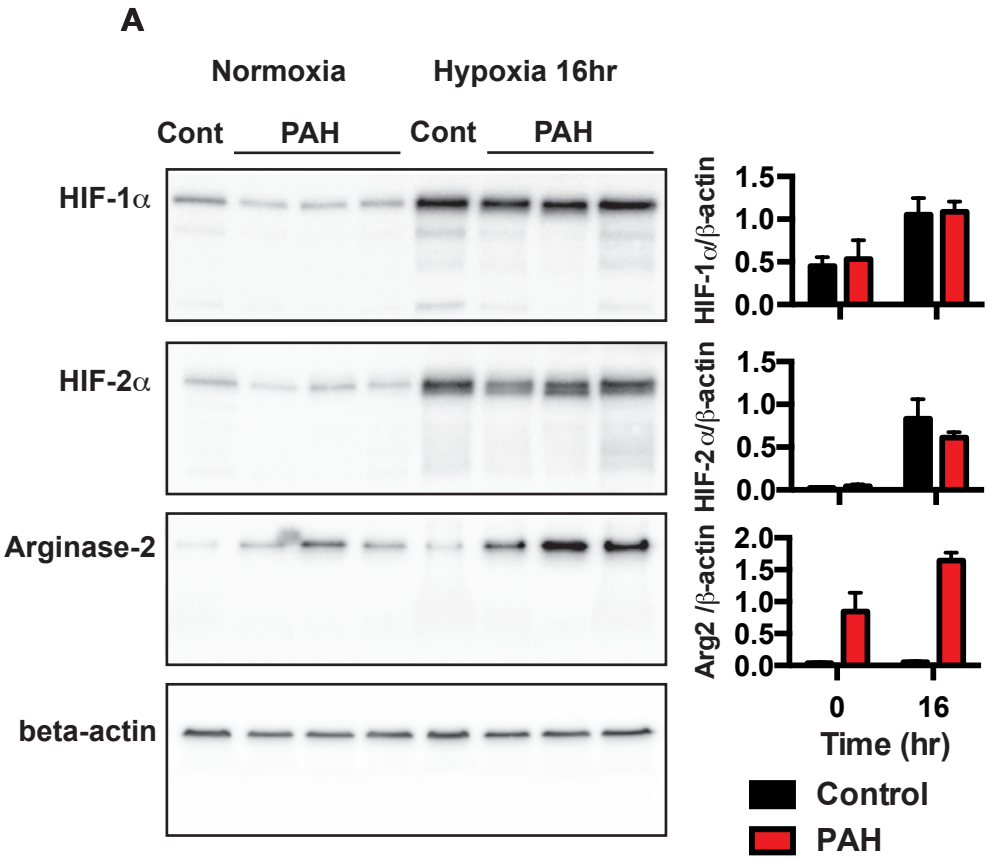
A
Normoxia
Hypoxia 16hr
Cont
PAH
Cont
PAH
HIF-1α
HIF-2α
Arginase-2
beta-actin
HIF-1α/β-actin
HIF-2α/β-actin
Arg2 /β-actin
1.5
1.0
0.5
0.0
2.0
0
16
Time (hr)
Control
PAH

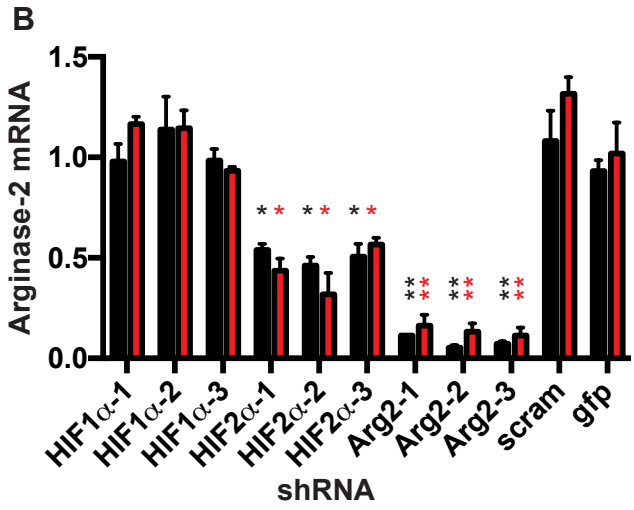
B
Arginase-2 mRNA
1.5
1.0
0.5
0.0
HIF1α-1
HIF1α-2
HIF1α-3
HIF2α-1
HIF2α-2
HIF2α-3
Arg2-1
Arg2-2
Arg2-3
scram
gfp
shRNA

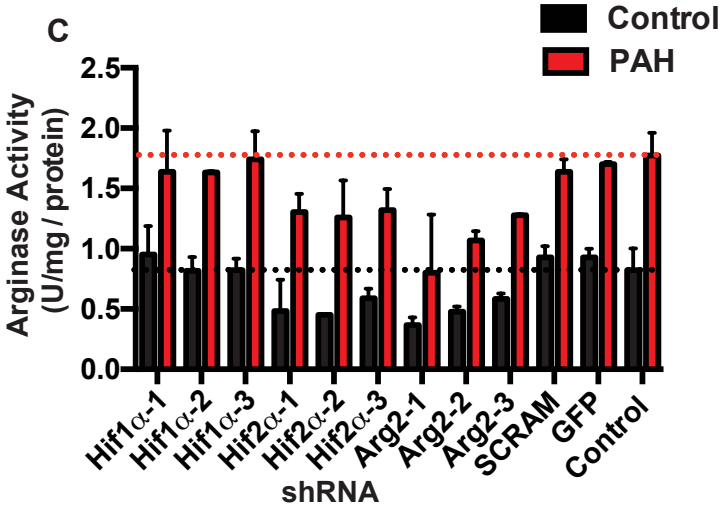
C
Control
PAH
Arginase Activity
(U/mg / protein)
2.5
2.0
1.5
1.0
0.5
0.0
Hif1α-1
Hif1α-2
Hif1α-3
Hif2α-1
Hif2α-2
Hif2α-3
Arg2-1
Arg2-2
Arg2-3
SCRAM
GFP
Control
shRNA

Supplemental Figure Legends

Supplemental Figure 1. L1cre specificity for pulmonary endothelial cells. Representative photomicrographs from 3 independent mice (A) show bright-field structure of frozen lung (cre- / cre+) heart (cre+), kidney (cre+) and liver (cre+) sections, immunohistochemistry staining red for podocalyxin (vasculature), green td-RFP (cre+ activity) and merged image. (B) L1cre deletion efficiency of HIF-2α in isolated pulmonary endothelial cells and other selected whole organs. Isolated endothelial data shown as single experiment from six pooled animals.

Supplemental Figure 2. Haematological and body weight response to chronic hypoxia, and a hypoxic time course of endothelial HIF1α □□□e□□□□. (A) Red blood cell counts (RBC), haemoglobin (HGB) scores and (B) white cell counts (WBC) did not deviate between the groups (A) Data shown as scatter graph as mean ± SEM of RBC, HGB and WBC from normoxic (N) and chronic hypoxic (H) housed wild-type (WT) (n=9 and n=15) L1cre-HIF-1α (n=9 and n=8) and L1cre-HIF-2α (n=7 and n=8). (C) Bar graph of mean ± SEM body weight, normoxic (N) and after chronic hypoxia (H) from WT (n=8), L1cre-HIF-1α (n=7) and L1cre-HIF-2α (n=8). Deletion of endothelial HIF1α did not modulate the development of right ventricular hypertrophy (D) or the accumulation of red-blood cells (E) compared to wt control throughout the hypoxic time course of 7-14-21days. Data shown as

scatter graph as mean ± SEM of RV/LV+S and RBC counts for WT (n=5-17) and L1cre-HIF-1α (n=5-13).

Supplemental Figure 3. Histological sections from paraffin wax embedded lungs were immunostained for αSmooth-Muscle actin, von Willebrand factor, and stained for hematoxylin & eosin and Elastic van Gieson (EVG). Representative photomicrographs show no remodelling in normoxic housed L1cre-HIF-1α or L1cre-HIF-2α mice when compared to wild-type control.

Supplemental Figure 4. Deletion of pulmonary endothelial HIF-2α or Arg-1 decreases collagen deposition around arteries associated with terminal bronchus. Histological lung sections were stained using Sirius red and then analysed by image J software. Data shown as bar graph for (A) wild-type (WT) (open bar, n=7), L1cre-HIF-1α (blue bar, n=6) and L1cre-HIF-2α (red bar, n=7) and (B) wild-type (open bar, n=5) and L1cre-Arg-1 (green bar n=6) and representative photomicrographs show the degree of collagen deposition following chronic hypoxic challenge. **P<0.001

Supplemental Figure 5. Arginase and Endothelin-1 expression in isolated pulmonary endothelial cells and whole lung. (A and B) QPCR data from a single experiment of six pool animals, pulmonary endothelial cells isolated from wild-type or L1cre-HIF-2α mice culture in normoxia or hypoxia for 24hrs. (C) QPCR analysis of ET-1 expression in whole lung tissue from wild-type (n=15), L1cre-HIF-1α (n=7) and L1cre-HIF-2α (n=6) mice following chronic

hypoxic challenge. (D) Acute hypoxic increase in plasma endothelin-1 was inhibited in the L1cre-HIF1α (n=4) and L1cre-HIF2α (n=4) mice when compared to wild-type (n=6). Plasma endothelin-1 was significantly lower in L1cre-HIF2α (n=8) compared to wt (n=8)following chronic hypoxic challenge Data bar shown as mean ± SEM. (E) Exhaled nitric oxide was measured non-invasively in non-anesthetised mice following chronic hypoxia, gas phase NO was measured by a chemiluminescence-based NO analyser. Data shown as scatter graph with mean ± SEM WT (n=6), and L1cre-HIF-2α (n=6) and L1-Arg1(n=5)*P<0.05.

Supplemental Figure 6. Endothelial deletion of HIFα does not influence the hypoxic modulated expression of PDGFα / β or PDGF-receptor A/B. QPCR data (fold change) for PDGFα / β and PDGF receptor A/B expression in whole lung from wt (n=8-16) (A and C) L1cre-HIF-1α (n=8) and (B and D) L1cre-HIF-2α (n=8). QPCR data (fold change) for stem cell markers nanog, oct3-4, klf4 and sox2 are shown for wt (n=8) and L1re-HIF2α (n=8). Data shown over a hypoxic time course 0-1-3-21 days. *P<0.05.

Supplemental Figure 7. Red blood cell counts (RBC), haemoglobin (HGB) did not deviate between the groups (A) Data shown as scatter graph as mean ± SEM of RBC and HGB from normoxic (N) and chronic hypoxic (H) housed wild-type (WT) (n=6(N) and 4(H)) L1cre-Arg1 (n=6 (N) and n=9(H)) (B) Histological sections of lung were immunostained with α–smooth-muscle actin(α-SMA), von Willebrand factor(vWF), and Elastic van Gieson (EVG). Representative photomicrographs demonstrate the remarkable attenuation of

remodelling in L1cre-Arg1 pulmonary arteries associated with terminal bronchi when compared to WT control

Supplemental Figure 8. Pulmonary respiratory response to acute hypoxia. (A,B and C) Minute volume, tidal volume and flow rate in response to hypoxia were determined by whole-body plethysmography. Data shown as mean ± SEM for wild-type (n=10), L1cre-HIF-1α (n=5) and L1cre-HIF-2α (n=6). Pulmonary endothelial HIF-2α does not influence carotid body development. (D and E) Representative photomicrographs showing immunostaining of TH^+ cells in the carotid bifurcation of wild-type (WT) (n=5) and L1cre-HIF-2α (n=5). To facilitate comparison, the areas inside the rectangles are shown at a higher magnification. ECA, external carotid artery; ICA, internal carotid artery; CB, carotid body; SCG, superior cervical ganglion. Scale bar 200μm and 20μm respectively. Quantification of (F) CB TH^+ cells, (G) carotid body volume, and (H) CB TH^+ cells per area of tissue.

Supplemental Figure 9. Analysis of human Blood Out-growth Endothelial Cells (BOECs) for arginase-2 expression, activity and NO synthesis. (A) qPCR analysis of arginase-2, data shown as mean ± SEM from control (open bar n=3) and PAH (red bar n=4), (B) arginase activity assay data shown as mean ± SEM from control (open bar n=4) ± arginase inhibitor (BEC)(black checker bar n=4) and PAH (red bar n=3) ± arginase inhibitor (BEC)(red and black checker), (C) NO analysis of whole cell lysates from BOECs cultured for 48hr. Data shown as mean ± SEM from control (open bar n=4) ± arginase

inhibitor (BEC)(black checker bar n=4) and PAH (red bar n=3) ± arginase inhibitor (BEC)(red and black checker).

A lentiviral short-hairpin RNA strategy was employed to target HIF1α, HIF2α and Arg-2. Three different shRNA were used to knock-down each gene of interest, including a scramble-sh and GFP-tagged lentivirus and no-treatment were included as controls. Data shown (mean ± SEM qPCR fold change compared to no-treatment control) for (A) HIF1α and (B) HIF2α from control (closed bar, n=3) and PAH (red bar, n=3) 16hr post hypoxia. **P<0.001 (control) **P<0.001(PAH).

Supplemental Methods

Blood outgrowth endothelial cells (BOEC) isolation culture.

BOECs have been extensively used as a model for studying in-vitro endothelial function in vascular disorders and we have previously demonstrated their close functional and gene expression similarity to pulmonary artery endothelial cells.

Participants were previously diagnosed with pulmonary arterial hypertension or normal health volunteers. Mononuclear cells were isolated from 60 ml of venous blood by Ficoll density gradient centrifugation and plated onto type 1 rat tail collagen–coated (BD Biosciences, Bedford, MA) flasks in endothelial selective medium (EGM2; Lonza Biologics, Slough, UK) supplemented with 10% ES-screened fetal calf serum and additional growth factors (EGM2 bullet kit; Lonza Biologics). BOECs appear after 2–3 weeks and were subsequently passaged when confluent. Inhibition of arginase-2 activity, BOECs were culture with S-(2-boronoethyl)-L-cysteine (BEC) 24h before analysis.

Arginase activity assay

BOECs were prepared from cell lysate (50uL) added to 75uL of Tris-HCl (50mmol/L, pH 7.5) containing 10 mmol/L $MnCl_2$. Heat lysate to 55^{o}C for 10 min. Add 50uL of arginase substrate (L-arginine 0.5mol/L. pH 9.7) at 37^{o}C for 1 hr. Reaction stopped by adding 200uL of acid solution (H_2SO_4:H_3PO_4:H_2O 1:3:7). For calorimetric determination of urea, α-□□□□□□□□□□□□ropiophenone (25uL, 9% in EtOH) was added to the mixture and heated to 100^{o}C for 45 min. After placing samples in dark for 10 min at RT the urea concentration was determined by spectrophotometry by

the absorbance at 550nm. Urea production was normalized with protein concentration.

Carotid Body Histology. Carotid bifurcations were dissected, fixed for 2 hours with 4% paraformaldehyde (Santa Cruz) and cryopreserved with 30% sucrose in PBS. 10 um-thick cryosections were obtained (Bright cryostat) and tyrosine hydroxylase (TH) positive cells were detected by immunofluorescence using rabbit anti-TH antibody (Novus bioscience ref: 300-109) and goat anti-rabbit Alexa568 antibody (Life technologies ref: A11036). Carotid body volume and cell numbers were quantified on microscope images (Leica DM-RB) using ImageJ software.

Whole Body Unrestrained Plethysmography. A single chamber plethysmograph (Data Science) was used in conjunction with a pressure transducer. This utilises the barometric analysis technique that compares the pressure difference between the animal chamber and a reference chamber to measure airway physiological parameters. Unanesthetized mice were randomly placed into the plethysmograph and allowed to acclimate. Baseline averages of breathing frequency, tidal volume, inspiration and expiration volumes/ times were recorded. Once acclimated to the chamber, the composition of the flow gas was switched from 21% O_2 to 10% O_2 using a PEGAS mixer (Columbus instruments). The mice were housed in the reduced oxygen environment for 60 min before being returned to atmospheric oxygen.

Oxygen Saturations. According to the manufacturers instructions, the measurement was done using MouseOx® Pulse Oximeter (Starr Life Sciences Corp).

Exhaled Nitric Oxide analysis

Exhaled nitric oxide was measured non-invasively in non-anesthetised mice using a closed chamber system. Briefly, gas phase NO was measured by a chemiluminescence-based NO analyser sensitive to 0.1ppb NO (NOA 280i Sievers, Boulder CO). For measurement of exhaled NO a single mouse was placed in a plexiglass chamber (300ml volume) and perfused with medical air (FIO_2=21%) at a flow of 200ml/min giving a final NOA280i cell pressure of 8Torr (8 mmHg). Exhaled NO was continuously recorded for 15 min. Analysis of the final 5min was used to determine the level of exhaled NO (ppb). Measurement of exhaled NO from chronic hypoxic mice followed the same protocol as above except the carrier gas was mixed for FIO_2=10%.

Whole Lung Nitric Oxide analysis

Lung nitrogen oxides (NOx) were isolated from 100 mg of homogenized tissue using a hypotonic lysis buffer and were centrifuged at 1,000 × *g*, 4 °C, for 5 min. All samples were analyzed for total NOx content using an NOA 280i (Siever, GE Healthcare) according to the manufacturer's instructions.

Primary Lung endothelial cell isolation

Primary endothelial cells were isolated and cultured from lungs of L1cre-HIF2α and wt mice. Briefly, the lungs were excised, minced, and digested for 90 min at 37°C in 2 mg/ml collagenase type I (Roche) in HBSS containing 2 mM $CaCl_2$, 2 mM $MgSO_4$, and 20 mM HEPES. The digest was filtered through a 70 µm nylon cell strainer and washed once in HBSS. Pellet was then resuspended in PBS containing 0.1% BSA and incubated with anti-CD31-coated magnetic beads (Dynal, Invitrogen) for 1 hr at 4°C. Separated cells and beads were plated in endothelial cell growth medium (ECGM)

consisting of low glucose DMEM:F12 with 1% penicillin/streptomycin, 1% nonessential aminoacids, 2 mM sodium pyruvate, buffered with 20 mM HEPES and containing 20% FBS (Omega Scientific, Tarzana, CA), 20 µg/ml Heparin (Sigma, St. Louis, MO), and 75 µg/ml endothelial mitogens (Biomedical Technologies).

Knockdown experiments.

Human blood outgrowth endothelial cells derived from both control and PAH donors were transduced using lentiviral particles containing three different short hairpin RNAs (shRNAs) targeting human HIF-1α, HIF-2α, and Arg-2 mRNA, respectively. shRNA sequences were selected from The RNAi Consortium (TRC) according with the following criteria: those shRNAs appearing to have less potential off-targets binding sites and that were validated by MISSION® shRNA Library (Sigma-Aldrich). The individual clones ID selected were: TRCN0000003808 (HIF1α-1), TRCN0000003810 (HIF1α–2), TRCN0000003811 (HIF1α-3), TRCN0000003806 (HIF2α-1), TRCN0000342501 (HIF2α-2), TRCN0000003805 (HIF2α-3), TRCN0000333446 (ARG2-1), TRCN0000369866 (ARG2-2), and TRCN0000363741 (ARG2-3). Oligos for each individual shRNA were annealed and cloned into pLKO.1 plasmid following TRC recommendations. Positive colonies were checked by sequencing. To produce lentiviral vectors, Lenti-X^{TM} 293T cells (Clontech) were co-transfected with single pLKO.1, pCMV-dR8.91 and pMD2.G plasmids using Lipofectamine 2000 (Thermo-Fisher Scientific) manufacturer's protocol. Lentiviral particles were collected 48 hours after transfection and used to transduce BOECs over night. Next,

fresh media was added and the cells were incubated in normoxia for 2 day then in 1% O_2 atmosphere for 16 hours.

Pulmonary Vascular Morphometry. Lung tissues were stained with hematoxylin and eosin, sirius red or elastic van Gieson (EVG) stain to assess morphology (all Merck/BDH, Lutterworth UK). To determine the degree of muscularization of small pulmonary arteries, serial lung tissue sections were stained with anti-smooth muscle α-actin (α-SMactin; DakoCytomation Ely UK) and von Willebrand factor (DakoCytomation). Antibody staining was visualised using 3-3' diaminobenzidine hydrochloride substrate (DakoCytomation) and counterstained with Carrazzi hematoxylin (Bios Shelmersdale UK). Tissue sections were independently coded by a third person before quantification of the sections. Vessel medial thickness was measured using Image J software (MediaCybernetics, Bethesda MD).

RNA Analysis. Total RNA and DNA was isolated from the lung using TRI-reagent (Sigma) followed by RNA clean-up and DNase digest using RNeasy column kits (Qiagen). First-strand synthesis was performed with 1μg of total RNA using a high-capacity cDNA kit (Applied Biosystems) according to the manufacturers instructions. Relative gene expression was determined by quantitative PCR (qPCR) (One-Step Plus Real-Time PCR System; Life Technologies) and was amplified in SYBR-Green master mix (Roche) and relevant primers from Qiagen. Relative gene-expression levels were related to β-actin and B_2M using the $2\Delta\Delta CT$ method.

Supplemental Figure 1

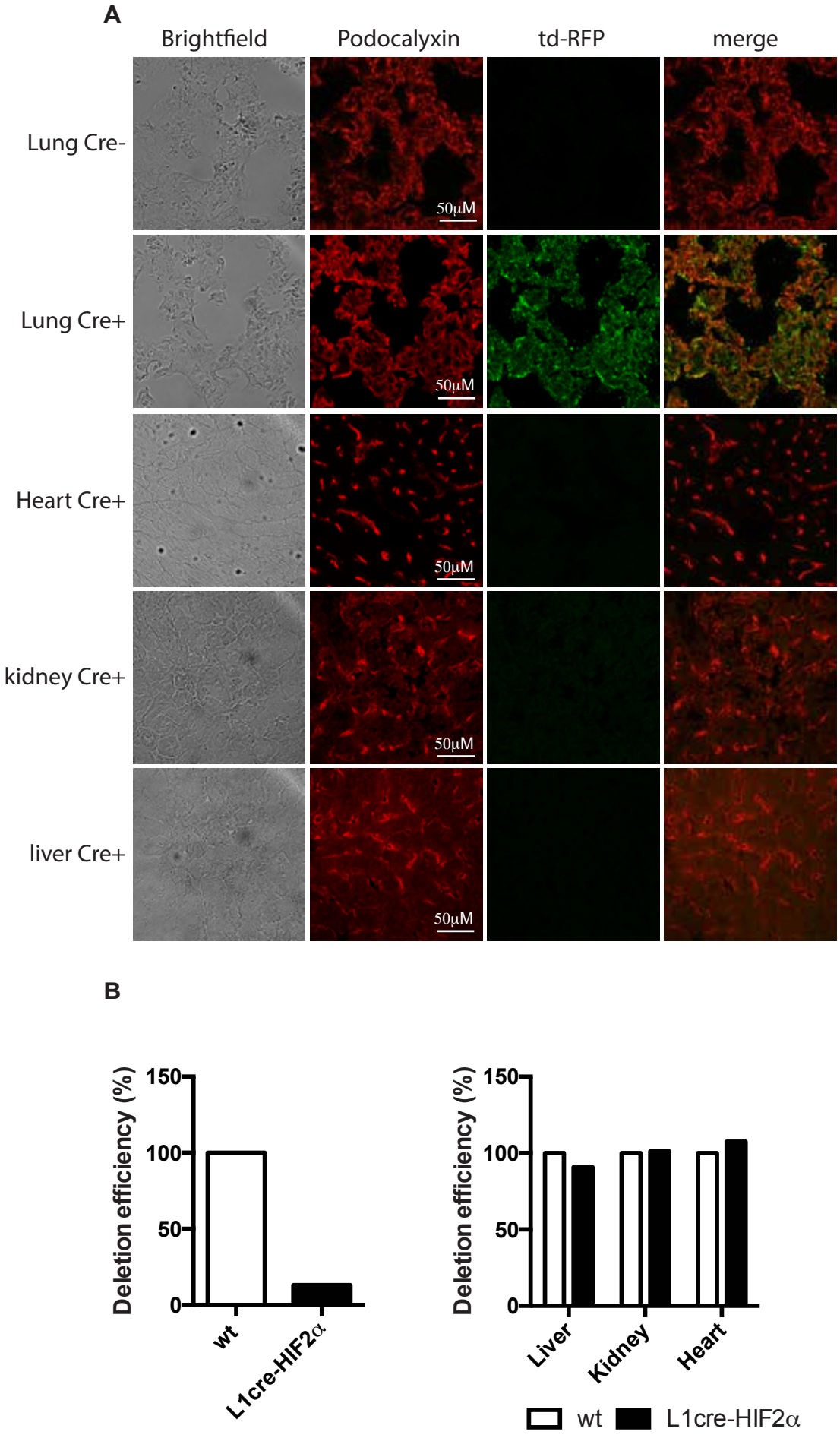

Supplemental Figure 2

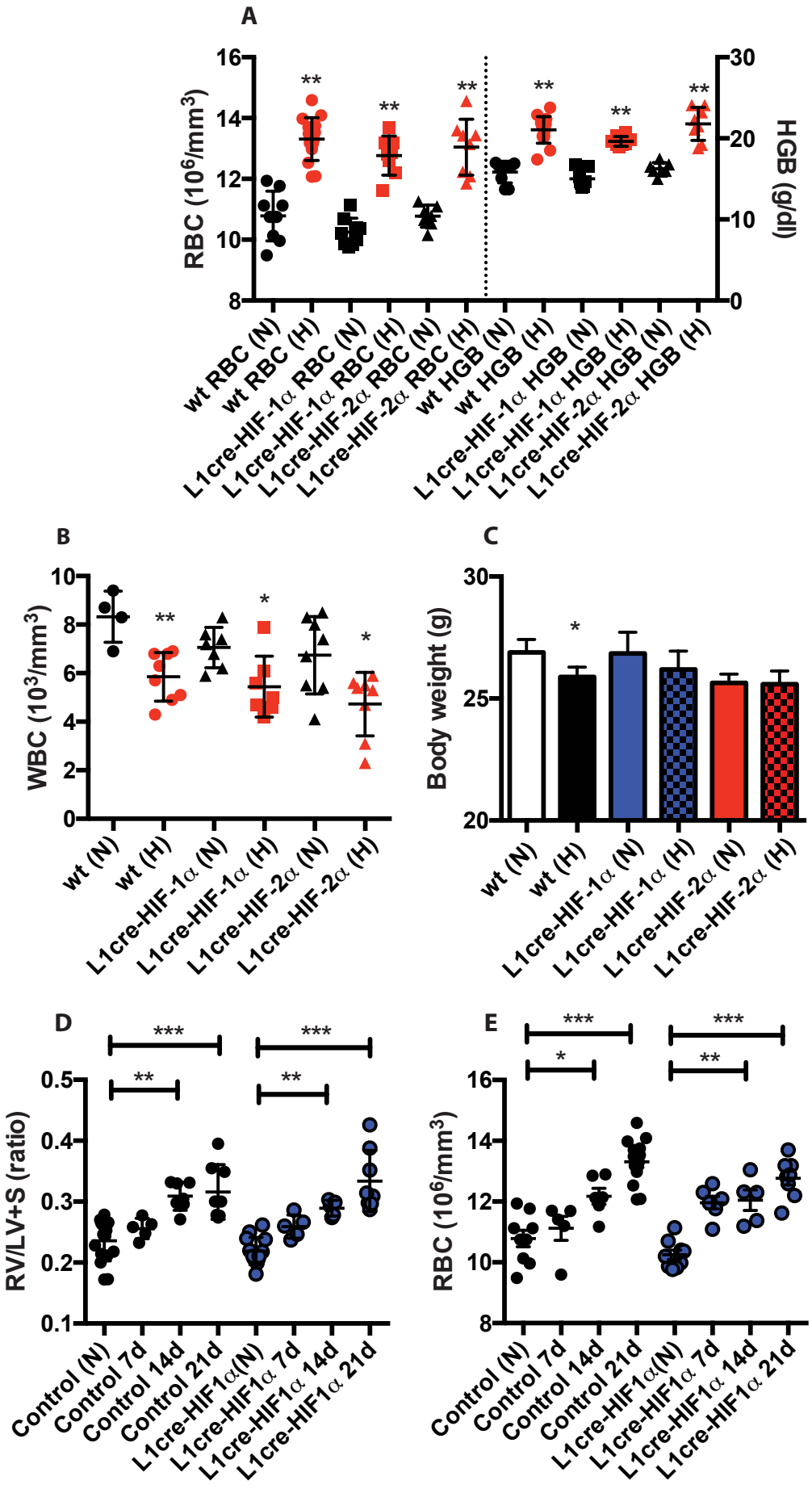

Supplemental Figure 3

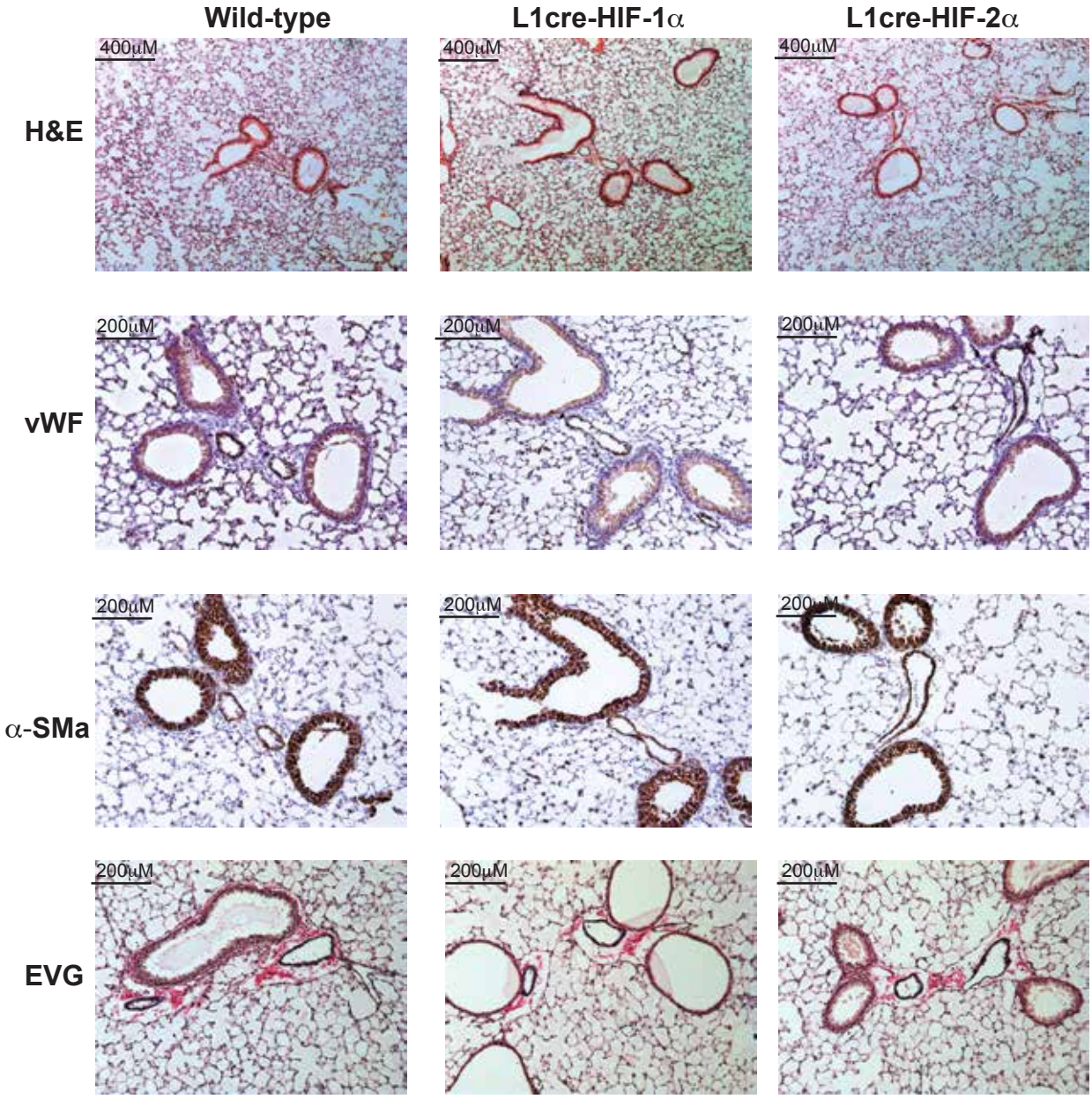

Supplemental Figure 4

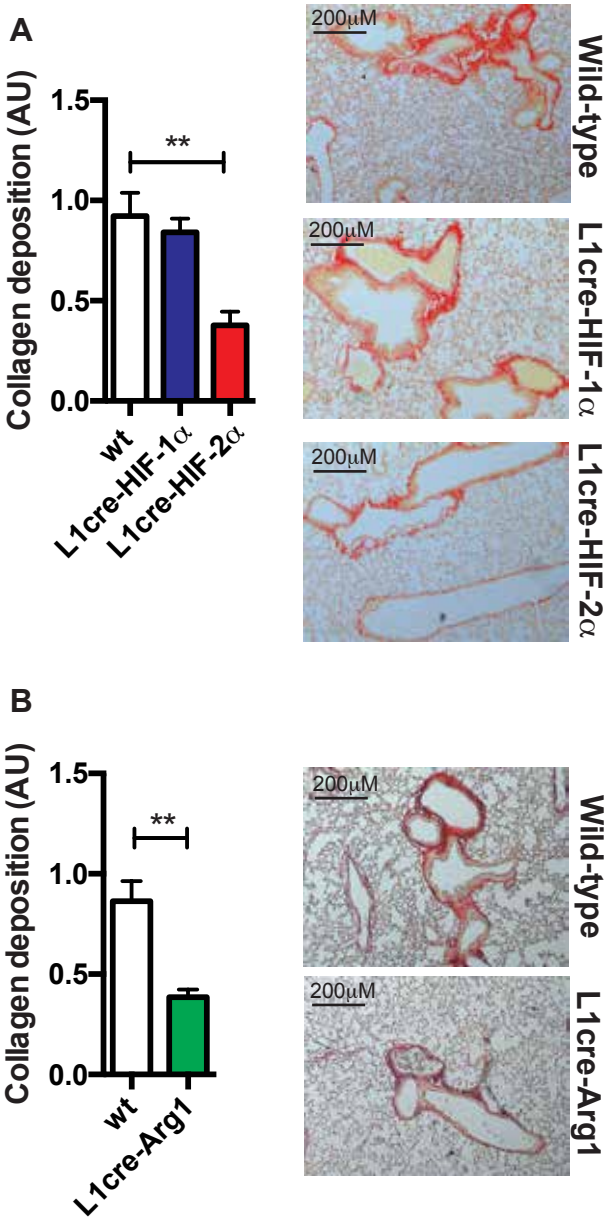

Supplemental Figure 5

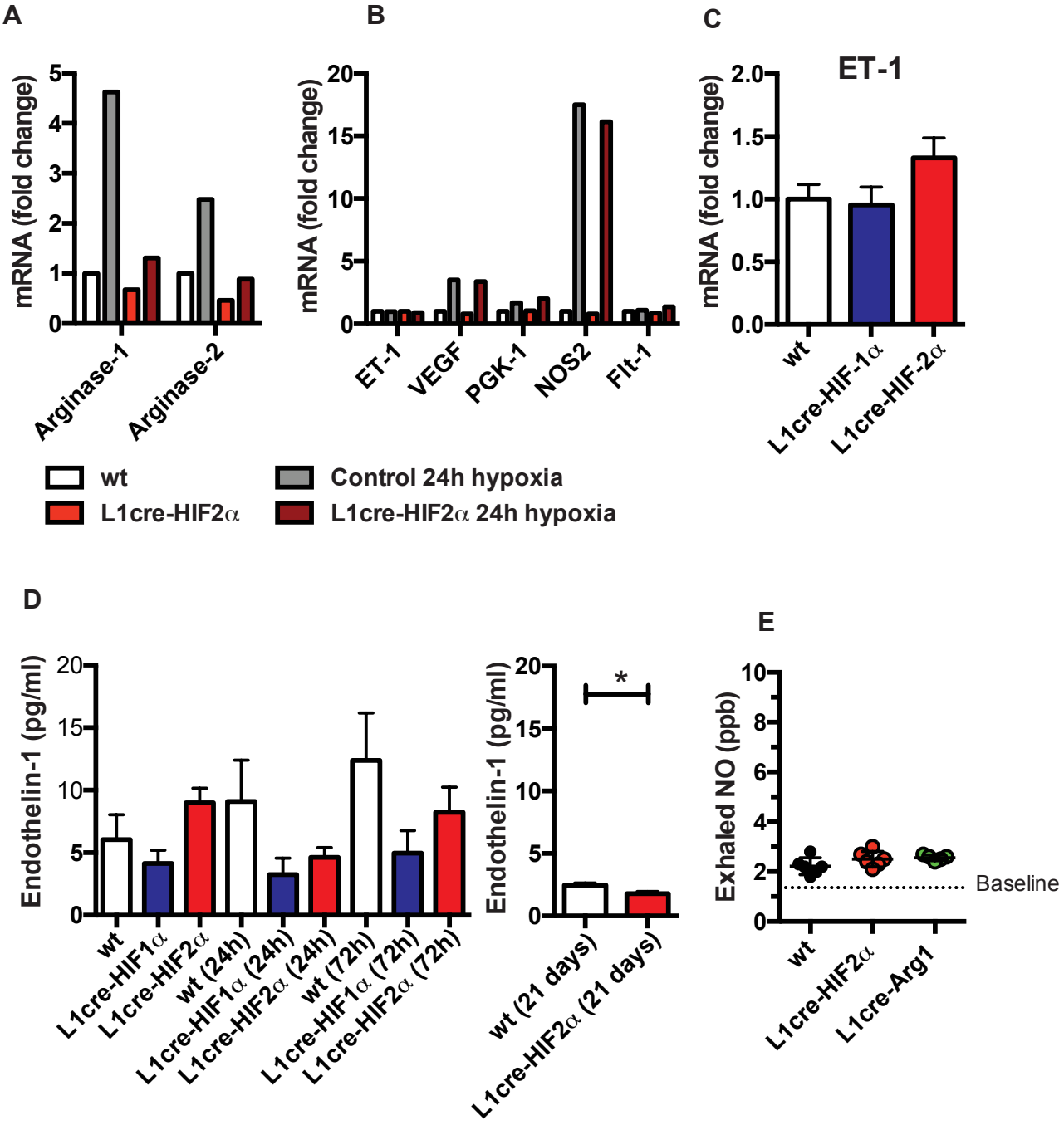

Supplemental Figure 6

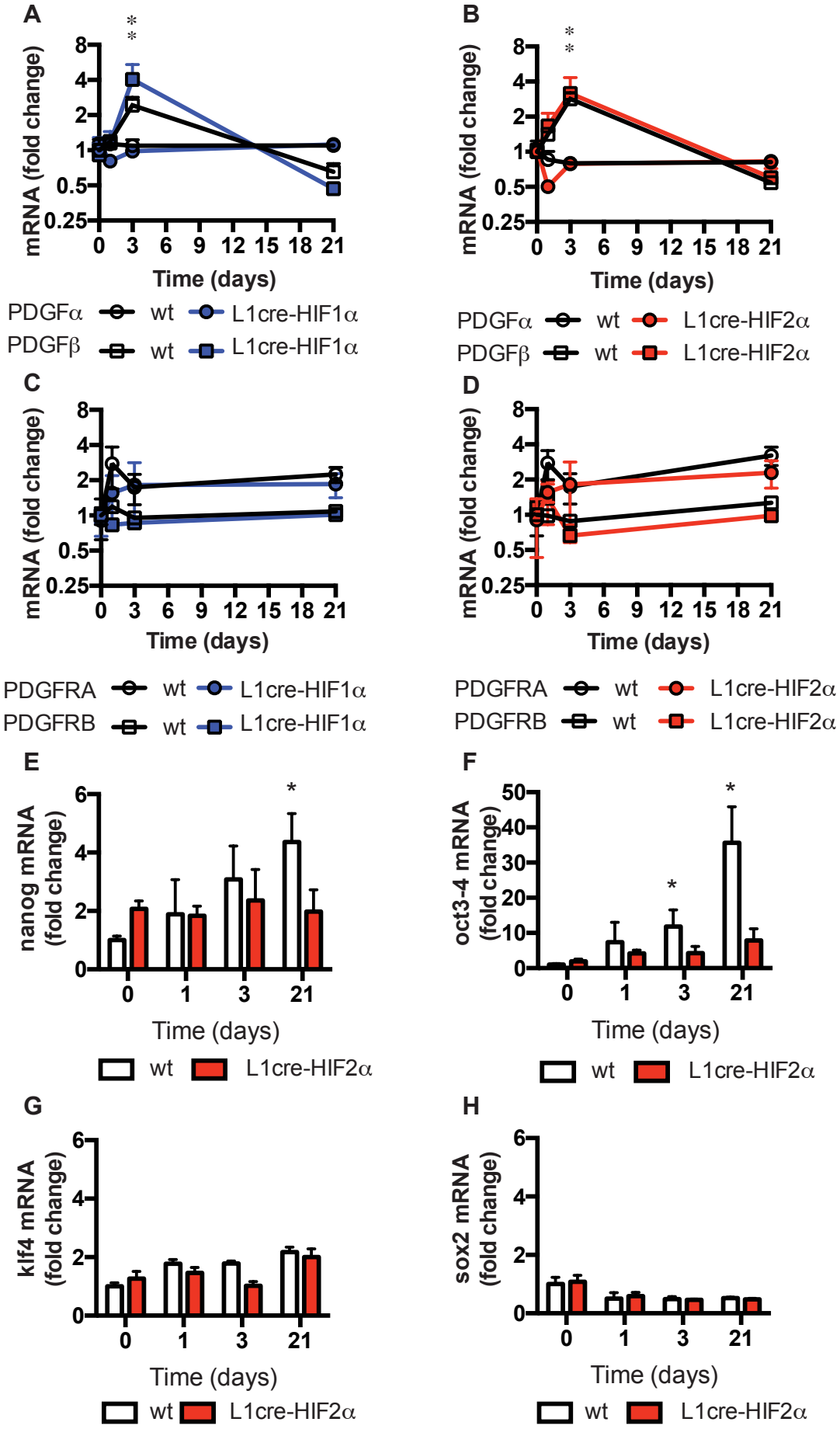

Supplemental Figure 7

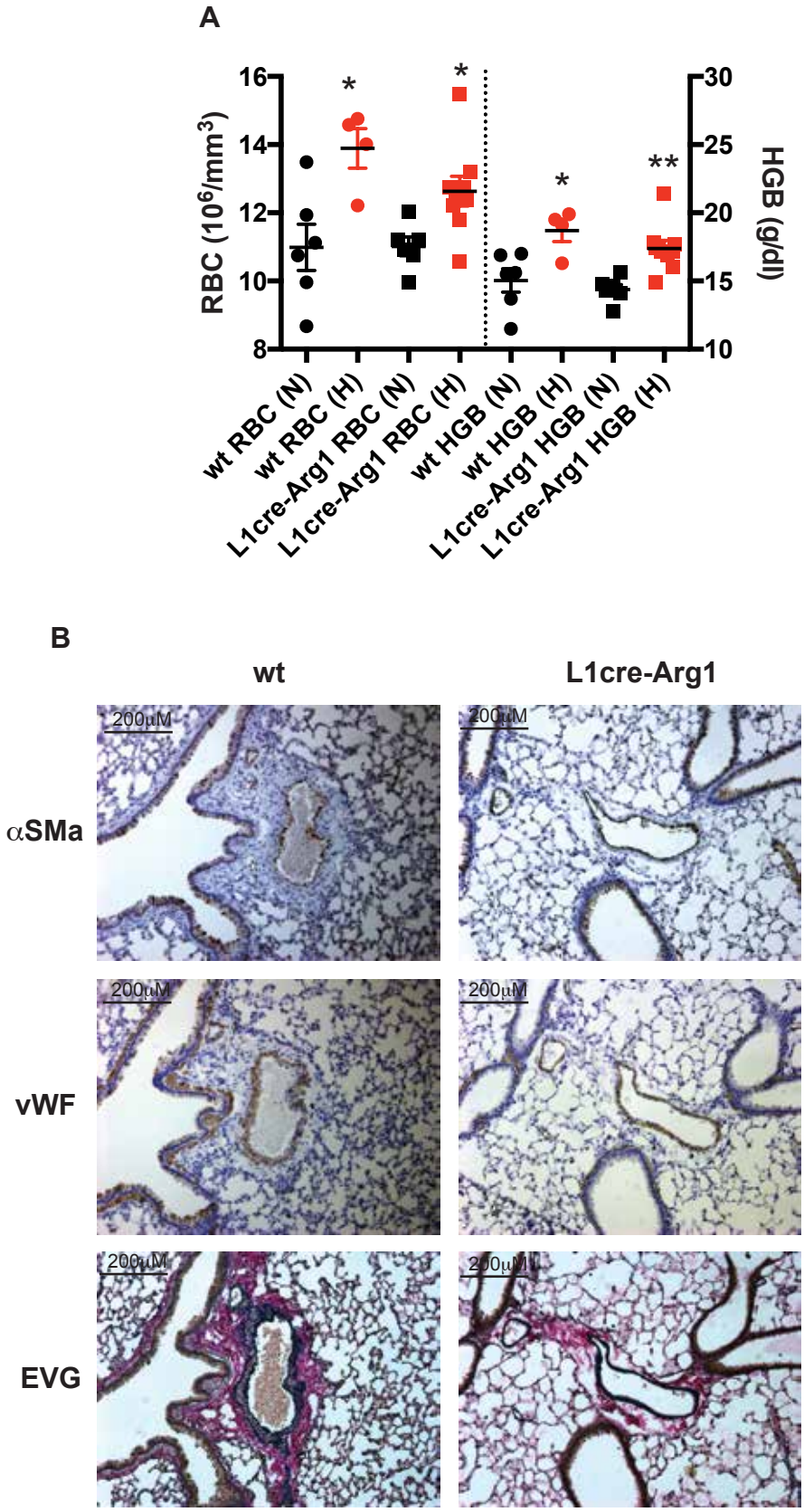

Supplemental Figure 8

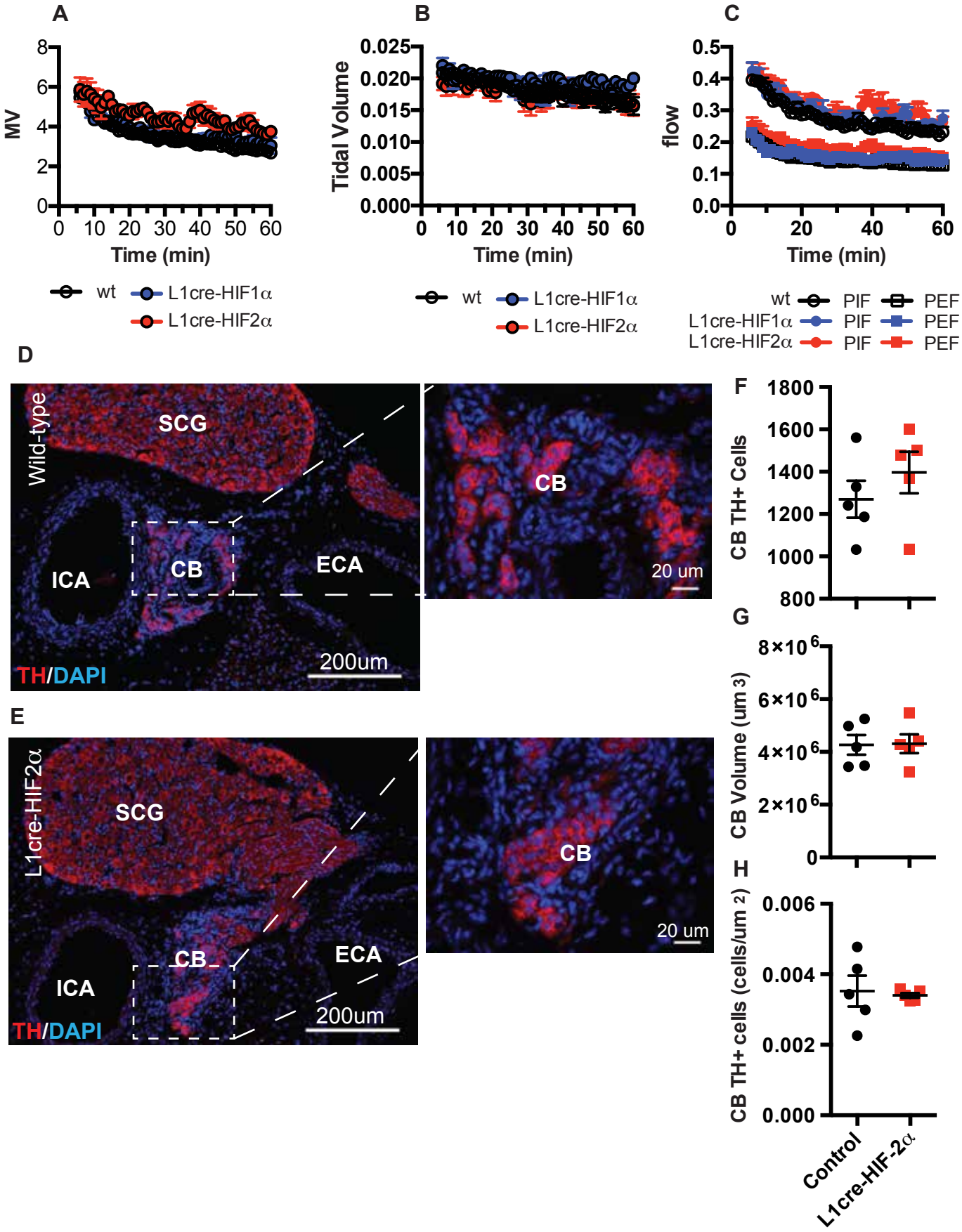

Supplemental Figure 9